Hygro-thermal model for estimation of demand response flexibility of closed refrigerated display cabinets

Applied Energy 284 (2021) 116381

Contents lists available at ScienceDirect

Applied Energy

journal homepage: www.elsevier.com/locate/apenergy

Hygro-thermal model for estimation of demand response flexibility of closed refrigerated display cabinets

Tommie Månsson *, Angela Sasic Kalagasidis, York Ostermeyer

Building Technology, Architecture and Civil Engineering, Chalmers University of Technology, Gothenburg, Sweden

ARTICLE INFO

Keywords:
Refrigerated display cabinet
Supermarket
Thermal modelling
Food retail
Energy efficiency
Demand response
Demand-side management
Renewable energy
Smart grid

ABSTRACT

In this article we present and validate a novel methodology for estimating the temperature development and heat extraction demand of closed refrigerated display cabinets (RDCs) in operating conditions, for near-future prediction and optimisation in smart grids. The approach is based on an in-house developed hygro-thermal model of an RDC, in which the conditions in each of the three main calculation domains, representing the internal air, heat exchanger and interior, are estimated at a temporal scale of seconds. The interior air temperature, heat extraction rate and run-off condensate were validated towards experimental data with good conformity. Moreover, for demand response purposes, in this article, we provide examples of how the model can be used to evaluate the temporal flexibility in heat extraction demand of RDCs. In a hypothetical supermarket with 11 RDCs exposed to various thermal loads and customer interactions, it is estimated that the heat extraction demand could be reduced to 0 for up to 83/127 s during opening/non-opening hours respectively. With a strategic pre-cooling, the latter time could be extended to 322 s. For the case of a demand response signal requesting the supermarket to absorb excess energy, all RDCs would be able to run at full power for up to 17/29 s, and approximately half of them for additional 20 s during opening hours. These findings are based on a total of 44 *five-minutes-ahead* simulations of possible scenarios for the 11 RDCs, all calculated by the presented model in approximately 10 s. In conclusion, the model provides fast and reliable results for real-time predictions in refrigeration control systems either for the benefit of the electrical grid by demand response or for energy efficiency purposes.

1. Introduction

By the year 2050, the European Union (EU) aims to reduce its release of greenhouse gases (GHG) by 80% – 95% compared with the levels in 1990 [1]. As a milestone, the EU should reach an overall share of 27% of renewable energy by 2030 according to the Revised Energy Directives (REDII) [2]. In several regions in the EU, energy efficiency measures and the replacing of fossil energy sources with solar, wind and wave power are strategies to decrease the release of GHG caused by energy generation. However, a large share of non-dispatchable or intermittent energy sources does create an issue for the utility grid to balance the supply and demand of energy. For years back, this is evident in Germany, where a high ratio of solar and wind power causes a surplus of energy at annually occurring events that cannot be distributed and utilised adequately, resulting in a negative tariff for electricity [3]. On the contrary, the intermittency also introduces an issue at times of insufficient power generation, causing a deficiency of available energy in the grid, resulting in increasing peak-tariffs [4]. Hence, measures must be taken to ensure the demand is realised for the end-users. However, instead of physically expanding the grid capacity to redistribute the surplus or compensate for the deficiency, demand-side flexibility could potentially mitigate this issue [5]. Thus, energy management strategies for both the generation- and demand-side must be developed to ensure the energy balance of the grid, while keeping the operating cost and environmental impact at a minimum [6].

Measures can be taken manually by turning off or reducing the electrical power demand by equipment to benefit the utilities, in exchange for an incentive such as a lowered tariff or exemption from a peak tariff. Alternatively, the grid balancing measures may be fully automated in a smart grid setting that comprises an adequate communication infrastructure for the exchange of data and control signals between utilities and end-users' equipment [7]. There are, however, challenges for controls and communication systems to overcome to meet the requirements of smart grids with a majority of the energy coming from intermittent sources [8]. One key aspects is the interoperability of the

* Corresponding author.
E-mail address: tommie.mansson@chalmers.se (T. Månsson).
URL: https://www.chalmers.se/en/staff/Pages/tommiem.aspx (T. Månsson).

https://doi.org/10.1016/j.apenergy.2020.116381
Received 14 August 2020; Received in revised form 10 December 2020; Accepted 20 December 2020
Available online 30 December 2020

Abbreviation

β	Moisture efficiency [−]
c_p	Specific Heat Capacity [J/kg K]
C	Heat Capacity [J/K]
CFD	Computational Fluid Dynamics
ΔH	Enthalpy of vaporisation [J/kg]
GHG	Green House Gases
h	Enthalpy [J/kg]
$HVAC$	Heating Ventilation and Air-Conditioning
K	Heat Transfer Coefficient [W/K]
$\dot{m}$	Mass flow rate [kg/s]
m	Mass [kg]
M	Molar Mass [kg/mol]
p	Pressure [Pa]
$\dot{Q}$	Heat flux [W]
RDC	Refrigerated Display Cabinet
S_i	Scenario i
T	Temperature [K]
t	Time [s]
W	Moisture ratio [kg/kg_{Dry}]
w	Weight/Constant [−]

Subscript

Amb	Ambient
$Cond$	Condensate
$DARA$	Mean Discharge and Return Air
$DARAG$	Mean Discharge and Return Air Grille
Dry	Dry air
Env	Envelope
Exf	Exfiltration
HE	Heat Exchanger
Inf	Infiltration
Int	Interior
RA	Return Air
RAG	Return Air Grille
Ref	Refrigeration
Sat	Saturated

communication platforms, which requires common standards defining how data are transferred and handled [9]. Here, OpenADR comprises a promising platform for the development and further deployment of demand response schemes.[10].

The two main categories for communication strategies from the side of the utilities are direct control and indirect control. For direct control, the end-user is requested to follow a power reference provided by the grid in exchange for an agreed incentive. For the indirect approach, a real-time price is communicated to incentives the end-users to adjust their power demand accordingly.

In the setting with an automated demand response operation, thermostatically controlled electrical loads are an area of particular interest as these loads represent a major part of electrical energy demand [11]. A common basis for thermostatically controlled loads is that the controlled processes allow fluctuations in temperature within a certain accepted range, without affecting the operation.

In the available literature, several approaches using the load shifting potential of thermostatically controlled resources have been proposed, e.g. by smart domestic appliances [12], electrical heating systems [13], hybrid solar-thermal domestic hot water systems [14], domestic refrigerators [15], and domestic air-conditioners [16]. The vast number of individual appliances and unique configurations does, however, cause a significant challenge for communication and estimation of actual capacity. Therefore, more energy intense industries and actors are beneficial to approach at first.

One large and energy-intense actor with a significant thermostatically controlled load is supermarket companies, and more precisely, their refrigeration systems in the stores [17], which at times of energy deficiency in the grid could be turned off rapidly [18]. The thermal inertia within the refrigerated display cabinets (RDCs) would allow the supermarket refrigeration system to be shut down for a limited period while the temperature of the refrigerated goods increases to an upper limit [19], making them suitable for fast responding direct load control. The refrigeration system does also have the possibility to absorb surplus electrical energy from the grid by transforming it into stored compressor work, i.e. by reducing the temperature of its refrigerated content.

Yet another aspect advocating for the utilisation of supermarkets for demand response purposes is the vast number of supermarkets, thus their electrical energy demand for their operations. As an example, on a national level, in Germany there are approximately 38 000 supermarkets with an accumulated energy demand of 10 TWh [20], which corresponds to an average annual power demand of 1.14 GW or 30 kW per supermarket. Hence, since approximately 50% of this energy demand originates from the refrigeration system [21], the average supermarket could potentially load-shift 15kW. In addition, a limited number of actors often represents a large share of the overall market, making it an addressable sector. In Germany, the four largest supermarket companies, namely Aldi, Netto, Lidl and REWE, represent 14 640 of the 38 000 stores [22]. Furthermore, as supermarket companies often have low-profit margins (2%–3%) [23], they are prone to adopt cost-reducing actions in their stores [24].

However, to enable supermarkets to engage and use their full potential for demand response purposes, smart grid communication possibilities together with detailed insights in the current and future temperature and heat extraction demand of the RDCs and their content must be predicted and controlled carefully [19,25]. This requires certain investments in updating the current control equipment [26]. Hence, this creates an initial cost for the supermarkets to engage in demand response, which must be covered by the cost-savings provided by the utilities. Therefore, detailed modelling is required to determine the precise capacity of supermarkets, and the actual value of the demand response service provided [27].

Ultimately, it is the temperature of the stored goods in the RDCs together with the power demand for refrigeration that determines the supermarkets demand response capacity. Modelling and control of RDCs energy performance in operational conditions is a developing area, hence a limited number of published works. In [25] the authors attempted to predict the product temperatures for demand response purposes. The methodology is based on an empirically derived relation between the openings of the expansion valve of the RDCs and the temperature of its content. Although the study is successfully validated, the model is limited to the test-case only and cannot take operational variations into account. For the implementation in a supermarket control system, accurate results for all possible operating scenarios are necessary. In addition, the models must be computationally efficient to allow for near-future predictions with the limited computational capacity of the control system.

Another, more flexible approach is numerical modelling methods such as computational fluid dynamics (CFD), which can provide the highest spatial and temporal resolution on temperature and air distribution in RDCs. They are, however, very computationally expensive [28], which makes them impractical for real-time applications and near-future predictions. An example of this can be found in [29] and [30], where the authors used a multi-scale approach to perform a stationary CFD simulation for a full supermarket with focus on the interactions

between HVAC system and RDCs. To enhance the computational performance of the CFD model, the authors separated the supermarket into three main spatial scales of interest; Sales area (> 10 m), RDC (1 m) and Shelves (1 cm). The resulting calculation time[1] was 60, 36 and 16 h respectively for the separate spatial scales. Consequently, for a more complex supermarket with several unique RDCs and shelves, the simulation time would be several days.

Although the number of stationary and transient CFD studies of RDCs is relatively large [31], examples of studies including the dynamic response of RDCs exposed to door openings such as [32] are rare. Within [32], each door opening event deforms the computational domain related to the RDC, which must be redefined, and a new mesh must be generated for each time-step. Consequently, the computational efforts increase substantially, making the time for calculation longer than the actual simulated time frame. Although this approach provided interesting results for the thermal loads by door openings, it is not applicable for real-time predictions because of the current limitations in computational performance.

For supermarkets' energy systems simulations, models that require limited computational effort to keep the total calculation time low when involving several RDCs are also needed. However, here the focus in the available literature is rather on the heat extraction rate than on the actual temperature of the RDCs and its content. In the building energy simulation software Energy Plus, the RDCs are modelled based on nominal performance parameters at rated conditions [33], which are combined with fixed relations to estimate their off-rated performance. For example, the variations between the day and night-time scenarios are described by a gain factor from [34]. In another software, Cybermart, the RDCs are modelled based on performances related to the indoor conditions as described in [35], in combination with the factors provided by [34] for day and night-time variations. The methods applied in both software do depict the average heat extraction demand of the supermarkets RDCs over larger temporal scales adequately. However, individual performance differences of RDCs are not included, limiting the insight into the spatial and temporal resolution of the results. The latter is also of interest for cold chain analysis. In [28], the authors studied the temperature development of goods being transported and stored at locations from a producer to end consumer, including the storage in open RDCs in a supermarket. For this study, they developed a heat transfer model to predict the steady-state conditions of the air and goods within an open RDC with a spatial resolution of two thermal zones per shelf [36]. This model was then further developed to include the transient temperature development for the goods [37], by using measured supply temperatures as input and by considering all products as isothermal objects. In the follow-up work [38], the authors adapted this transient model to be applicable for RDCs equipped with doors. However, this model does not consider the infiltration caused by door openings, which according to [19] is the main contributor for short term variations in heat extraction rates by RDCs in operational supermarkets.

Based on the presented literature review and to the best of our knowledge, no previously published model is capable of predicting the near-future temperature development and heat extraction rate of a closed RDC accurately and at a low computational cost, while considering the variations caused by door operations.

By being able to predict the near future temperature development and heat extraction demand, it is possible to estimate for what duration of time the RDC could be turned off or ran at an increased capacity without overheating or sub-cooling the content, which is necessary for demand response purposes. Therefore, to evaluate and enable the demand response potential in RDCs in supermarkets and support further development of energy-efficient supermarkets, we have developed a validated, accurate and computationally affordable model that predicts the temperature development of three main domains within the RDC with a temporal resolution of seconds.

[1] Simulations performed on a Dell server with Intel Xeon E5630 eight cores running at 2.53 GHz with 16 GB RAM [29].

2. Coupled heat and mass transfer balance model of a doored RDC

The main objective of the model presented in this article is to estimate the heat extraction and temperature development of a fully operational RDC and use these results as control parameters in the associated refrigeration system for demand response purposes or, alternatively, for optimised short-time scheduling of cooling cycles and improved energy efficiency. The model must be designed to run with a minimal computational effort while still providing accurate results in order to achieve this goal with the limited computational capacity of the control systems computer. Following the design of current control systems for RDCs and as a balance between spatial details, accuracy and computational cost, the spatial resolution of the model was limited to calculate the discharge air temperature T_{DA} and return air temperature T_{RA}, based on the temperature of the heat exchanger T_{HE} (Evaporator). In addition, as the model takes latent loads into account, the moisture content at these locations is also calculated, as well as the overall heat extraction rate and run-off condensation amount from the evaporator.

To enable prediction of near-future developments, the model operates in two modes, namely *Thermostat-mode* and *Tracking-mode*. In *Thermostat-mode*, the model adapts the heat extraction on the basis of an emulated thermostat control system, whose goal is to keep the temperature of RDC within the prescribed limits. Thus, when the upper temperature limit is reached, the heat extraction by the evaporator is activated until the lower limit is reached, and the RDC starts to heat up again. When the model is running in *Tracking-mode*, it is instead set to follow a real-time temperature signal from an actual RDC by simultaneously adjusting the heat extraction rate, based on the model described in Eq. (15). Thus, if the model is running in *Tracking-mode* following the measured T_{DARA} temperature, it will estimate the state of all domains of the RDC based on this trace. Thus, by using the generated data on the state of the domains from *Tracking-mode* as initial input for the model ran in *Thermostat-mode*, near-future predictions can be made. In these predictions, the RDC can be exposed to assumed scenarios, a variety of door openings, changes in ambient condition etc. More details and an example of how the model is used for near-future predictions are further described in Section 5.

The model comprises three main calculation domains as shown in Fig. 1, where the individual domains represent the air in the gross volume of the RDC, the thermal mass of the interior, and the heat exchanger (*Evaporator*) for the refrigeration system. These domains are thermally coupled by the circulating air, which changes its temperature and moisture content when moving from one domain to another. The discharge air from the heat exchanger (*Position 0*) enters the RDC-gross volume domain (*Position 1*), where thermal and moisture loads increase its temperature and humidity to levels represented by T_{RAG} and W_{RAG} (*Position 2*). The air then passes the circulation fans (*Position 3*), which further increases its temperature to T_{RA}, before it enters the heat exchanger domain where its temperature and moisture content are lowered to T_{DA} and W_{DA} (*Position 4/0*), through heat extraction (*Cooling and Condensation*) by the refrigeration system. The temperature and moisture content of the circulating air are found from the heat and mass balance equation described hereafter.

2.1. Moisture balance for RDC

A substantial amount of air infiltrates to the RDC because of air leakages and door openings, affecting the mass balance of moist air for the RDC. Therefore, both the sensible and latent thermal loads are also affected. As the enclosed air volume by the RDC envelope is constant and the pressure equalise through gaps between doors almost instantly, the mass balance of the RDC can be assumed to be at equilibrium at any given time. Hence, the exfiltrating mass flow of humid air ($\dot{m}_{Exf}$) can be defined as a difference between the infiltrating mass flow ($\dot{m}_{Inf}$) and the mass flow of water vapour that is condensed and transported out from the RDC in liquid form ($\dot{m}_{Cond}$), as shown in Eq. (1). The

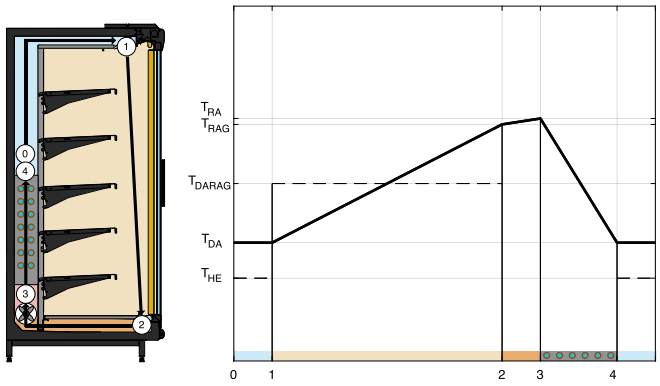

Fig. 1. Showing the domains and main temperatures evaluated within the model. *Left*: The RDC depicted with arrows indicating the flow direction and order. *Right*: Conceptual line graph showing the temperature development for the circulating air within the RDC.

Table 1
Input parameters representing the *Carrier Monaxis 63.C3 DL* at the conditions present during the validation experiment.

Parameter	Value	Unit
K_{Env}	40.15	[W/K]
$m_{RDC,Dry}$	7.69	[kg]
T_{Amb}	24/25	[° C]
W_{Amb}	$6.54 \cdot 10^{-3}$	[kg/kg$_{Dry}$]
$\dot{m}_{Inf}$	0.0412	[kg/s]
$m_{Opening}$	1.53	[kg/*opening*]
$\dot{Q}_{Lights}$	183	[W]
$\dot{Q}_{Fans}$	54	[W]
$\dot{m}_{Fans,Dry}$	0.55	[kg/s]
β	0.80	[−]
$\dot{Q}_{Ref}$	5750	[W]
C_{HE}	54 613	[J/K]
K_{HE}	600	[W/K]
C_{Int}	252 000	[J/K]
K_{Int}	392.5	[W/K]

determination of the mass flow rate of condensed water vapour, $\dot{m}_{Cond}$, is described in Section 2.3.

$$\dot{m}_{Inf} - \dot{m}_{Exf} - \dot{m}_{Cond} = 0 \leftrightarrow \dot{m}_{Exf} = \dot{m}_{Inf} - \dot{m}_{Cond} \tag{1}$$

For an RDC with closed doors, the infiltration mass flow rate through gaps is assumed constant, $\dot{m}_{Inf} = \dot{m}_{Inf,0}$, and given as a user-defined input based on the characteristic of the RDC. When the door is operated, the infiltrating mass flow rate increases to $\dot{m}_{Inf} = \dot{m}_{Inf,0} + \dot{m}_{Opening}$, where the user-defined $\dot{m}_{Opening}$ represents the additional infiltration through the opening. Both user-defined values were evaluated based on experimental data, generated by following the methodology presented in [39]. Alternatively, the necessary data on infiltration can be generated via other experimental methods or through calculations. Within the model, the infiltration to the RDC is defined as shown in Eq. (2).

$$\dot{m}_{Inf} = \begin{cases} \dot{m}_{Inf,0} + \dot{m}_{Opening} & \text{while door is open} \\ \dot{m}_{Inf,0} & \text{otherwise} \end{cases} \tag{2}$$

The moisture balance of the RDC is described in Eq. (3), which calculates the moisture ratio at the point of the return air grille, W_{RAG}. The inertia of the accumulation term on the left side comprises the capacity of the gross air volume of the RDC only, $m_{RDC,Dry}$. Any moisture buffering capacity of internal surfaces is neglected in this model but could be included as an additional term representing e.g. the interior or food goods. For vapour-tight packages of food goods, this buffering capacity is, however, negligibly small.

For the exfiltrating air, the mean moisture ratio of the RDC, $W_{DARAG} = (W_{DA} + W_{RAG})/2$ is used, assuming a perfect mixing within the RDC and uniform exfiltration. For the infiltrating air from the indoors, the ambient moisture ratio (W_{Amb}) applies.

$$m_{RDC,Dry}\frac{\mathrm{d}W_{RAG}}{\mathrm{d}t} = \dot{m}_{Inf,Dry}W_{Amb} - \dot{m}_{Exf,Dry}W_{DARAG} - \dot{m}_{Cond} \tag{3}$$

2.2. Heat balance for the RDC

The heat transfer within the model is based on the heat balance of the gross volume of the RDC coupled to the enthalpy of the circulating air at the point of the return air grille, h_{RAG}. In Eq. (4), the accumulation term on the left side represents the change of internal energy of the air in time, considering the latent loads from the condensed moisture.

In [40], the authors found that the heat transfer by radiation from the ambient to the RDC contributes to approximately 1.3% of the overall thermal loads when the doors are operated. This contribution is considered negligibly small, and the thermal loads caused by radiation is, therefore, excluded from the overall heat balance of the RDC.

$$m_{RDC,Dry}\frac{\mathrm{d}h_{RAG}}{\mathrm{d}t} = \dot{Q}_{Env} + (\dot{Q}_{Inf} - \dot{Q}_{Exf}) + \dot{Q}_{Lights} + \dot{Q}_{Int} - \dot{Q}_{HE} \tag{4}$$

The sensible heat gains to the RDC due to transmission through its envelope, including the glass doors, are calculated as shown in Eq. (5). Here, K_{Env} is the overall heat transfer coefficient of the airtight envelope. This constant can be evaluated either through calculations based on the geometry and materials of the RDC envelope or through experiments. In this study, K_{Env}, was evaluated following the Co-Heating method as described in [39].

$$\dot{Q}_{Env} = K_{Env}(T_{Amb} - T_{DARAG}) \tag{5}$$

The expression $(\dot{Q}_{Inf} - \dot{Q}_{Exf})$, as described in Eq. (6), represents the effects of infiltration of ambient air to the RDC. Here it is assumed that no mixing occurs in the close proximity of the RDC, i.e. the infiltrating air moisture ratio and temperature are equivalent to the ambient conditions. For the exfiltrating air, the air inside the RDC is assumed to be mixed homogeneously, i.e. analogous to the mass balance for moisture, $h_{DARAG} = (h_{DA} + h_{RAG})/2$.

$$(\dot{Q}_{Inf} - \dot{Q}_{Exf}) = \dot{m}_{Inf,Dry}h_{Amb} - \dot{m}_{Exf,Dry}h_{DARAG} \tag{6}$$

The term $\dot{Q}_{Int}$ from Eq. (4) represents the sensible heat transfer between the circulating air and domain representing the interior of the RDC, i.e. shelves and interior cladding in contact with the air inside the RDC. This heat exchange is further described in Eq. (7), where the temperature of the interior, T_{Int}, is calculated based on the transient balance shown in Eq. (8).

Thus, the term K_{Int} in Eq. (8) represents the convective heat transfer coefficient for the internal surfaces.

$$\dot{Q}_{Int} = K_{Int}(T_{Int} - T_{DARAG}) \tag{7}$$

$$C_{Int}\frac{dT_{Int}}{dt} = K_{Int}(T_{DARAG} - T_{Int}) \tag{8}$$

The interior comprises coated metal shelves and metal cladding covering the envelope's insulation, all of which are assumed to have a uniform temperature. For the RDC used in this study, Table 1 summarises the assigned parameters. Based on these parameters, the domain that represents the interior was found to have a time constant of $t_c = 642$ [s], which is considered significant in comparison to the duration of the compressor cycles (*approximately* 355 [s]).

2.3. Heat and moisture balance for the heat exchanger

The heat exchanger domain (Evaporator) represents a significant part of the heat capacity of the RDC. In contrary to the domain representing the interior, the heat exchanger domain is faster to respond with a time constant, $t_c = 90$ [s].

The heat extraction by the heat exchanger in the RDC, $\dot{Q}_{HE}$ from Eq. (4), is estimated as shown in Eq. (9).

$$\dot{Q}_{HE} = \dot{m}_{Fans,Dry}(h_{RA} - h_{DA}) \tag{9}$$

Where h_{RA} is the enthalpy of the return air just before entering the heat exchanger. This enthalpy is slightly higher than h_{RAG} because of the heat dissipated by the fans to the passing air as described Eq. (10):

$$h_{RA} = h_{RAG} + (\dot{Q}_{Fans}/\dot{m}_{Fans}) \tag{10}$$

The discharge air enthalpy, h_{DA} and $\dot{m}_{Cond}$, is calculated in three steps. First, the de-humidification of the return air is estimated by Eq. (11), where β represents the moisture transfer efficiency and $W_{HE,Sat}$ is the saturation moisture ratio at the temperature of the heat exchanger. Within the model, the moisture efficiency was assumed to be $\beta = 0.80$, and $W_{HE,Sat}$ was estimated from tabulated values presented in [41].

$$W_{DA} = W_{RA} - \beta \cdot (W_{RA} - W_{HE,Sat}) \tag{11}$$

In the second step, the mass flow rate of condensed water vapour is calculated by Eq. (12).

$$\dot{m}_{Cond} = \dot{m}_{Fan,Dry}(W_{RA} - W_{DA}) \tag{12}$$

Then, in the last step, the heat transfer from the return air to the heat exchanger is deducted from the discharge air enthalpy as shown in Eq. (13).

$$h_{DA} = c_{p,Air}(T_{RA} - 273.15) + W_{DA}(\Delta H_{Vap} + c_{p,Water}(T_{RA} - 273.15)) - K_{HE}(T_{RA} - T_{HE}) \tag{13}$$

Based on the above, the heat extraction rate $\dot{Q}_{HE}$ can be estimated and used in the calculations of the temperature of the heat exchanger, T_{HE} as described in Eq. (14). Here, $\dot{Q}_{Ref}$ represents the heat extraction rate by an arbitrary refrigeration system, controlled by a thermostat function, as described in Section 2.4.

$$C_{HE}\frac{dT_{HE}}{dt} = \dot{Q}_{HE} - \dot{Q}_{Ref} + \dot{Q}_{Adjust} \tag{14}$$

The term $\dot{Q}_{Adjust}$ represents a fictitious heat source or sink to force the model to follow a specific temperature if being operated in *Tracking-mode*. As an example, if the model is set to follow the measured T_{DARAG}, the adjustment term can be written as shown in Eq. (15).

$$\dot{Q}_{Adjust,DARAG} = K_{Adjust}(T_{DARAG,Input} - T_{DARAG,Model}) \tag{15}$$

The model then adjusts the heat exchanger temperature to force the temperature calculated by the model ($T_{DARAG,Model}$) to follow the given input data ($T_{DARAG,Input}$). The other model output such as discharge air temperature, return air temperature, condensate flow, and heat extraction can then be used for validation or error control while the model is in *Thermostat-mode*, $\dot{Q}_{Adjust} = 0$.

2.4. Heat extraction by the refrigeration system

The heat extraction rate $\dot{Q}_{Ref}$ is controlled by a thermostat control loop with an assigned constant heat extraction capacity of 5750 [W]. The control system activates the heat extraction once the temperature, $T_{Control}$, reaches the upper limit, T^{+}_{Set}, and continues to extract heat until a lower limit, T^{-}_{Set}, is reached. $T_{Control}$ is evaluated as expressed in Eq. (16) in the model as well as within the control system used in the validation experiments. For both, the weights were set to $w_1 = w_2 = 1$.

$$T_{Control} = \frac{w_1 \cdot T_{RAG} + w_2 \cdot T_{DA}}{w_1 + w_2} \tag{16}$$

To mimic the behaviour of the control system in the experimental setup, the thermal response time of the temperature sensors must be modelled. The temperature sensor tip comprises a 5 mm probe with a $t_c = 10$ [s]. For $T_i = T_{RAG}$ *or* T_{DA} the measured temperatures as perceived by a temperature sensor can be estimated as shown in Eq. (17), where $\frac{C}{K} = 10$ [s].

$$C_{i,Sensor}\frac{dT_{i,Sensor}}{dt} = K_{i,Sensor}(T_i - T_{i,Sensor}) \tag{17}$$

However, the irregular measurement errors and disturbances that occur in the experimental setup cannot be predicted because of their stochastic nature. Therefore, the impact of these variations cannot be included in the model.

2.5. Properties of moist air

The pressure in and around the RDC is assumed to be constant at $p_0 = 101\ 325$ [Pa] and the saturation vapour pressure, p_{vs} is found via interpolation from values listed in [41]. The actual vapour pressure is then calculated as shown in Eq. (18).

$$p_V = \frac{p_0 W_i}{(Mv/Ma) + W_i} \tag{18}$$

The enthalpy is calculated as shown in Eq. (19) following [41] where, $c_{p,Air} = 1\ 006$ [J/kgK], $c_{p,Water} = 1\ 860$ [J/kgK] and $\Delta H_{Vap} = 2\ 501\ 000$ [J/kg].

$$h_i = c_{p,Air}(T_i - 273.15) + W_i(\Delta H_{Vap} + c_{p,Water}(T_i - 273.15)) \tag{19}$$

The expression in Eq. (19) can be rearranged to calculate the temperature based on the enthalpy and moisture ratio of the air as shown in Eq. (20).

$$T = \frac{h_i - W_i \Delta H_{Vap}}{c_{p,Air} + W_i c_{p,Water}} + 273.15 \tag{20}$$

3. Validation and sensitivity analysis

For the validation of the model, an experimental setup with a *Carrier Monaxis 63.C3 DL* was arranged in a laboratory environment. Motors were attached to the door to mimic user interactions by door openings. Fig. 2 shows the dimensions of the RDC together with the location of the sensors used for collecting data on temperature and moisture ratio. Here, the door openers can also be seen mounted on top of the RDC.

The heat extraction rate was evaluated by measuring the mass flow, temperature and pressure of the refrigerant according to the setup described in ISO-23953:2 [42].

The mass flow of condensed water vapour was measured by connecting the drainpipe from the RDC to a reservoir where water was accumulated. A floating switch controlling an evacuation pump was triggered once 500 ml of water had been collected in the reservoir. The pump then evacuates the water through a flow meter where the volume was measured more precisely. This system allows evaluation of the average mass flow rate between the evacuation cycles with an accuracy of $< 2\%$, whereas the temporal granularity of the data becomes coarse ($\approx 1\ h^{-1}$) because of the size of the reservoir.

The validation experiment was conducted over 2 days. On the first day, all equipment was installed and the RDC was started to ensure a stable temperature during the measurement period. On the second, the data logging system was activated and data were collected for 10 h 20 min. During the first 4 h 35 min of data acquisition, the RDC doors were opened 6 times per hour per door, i.e. 36 openings per hour for the RDC.

The door operations executed by the motors were programmed to open the door blades to 90° at a speed of 45 °/s, then hold that position for 20 s before closing it at the same speed, resulting in a total duration of 24 s for a complete door opening. After the period of door operations, all doors were left closed and the data were collected for the RDC at idle state for another 5 h 45 min.

To give an overview of the full experiment, Fig. 3 shows the measured return, discharge and interior air temperatures during the full experiment. Here, the increased variations in temperatures during the period of door operations are shown. For a more detailed view of the temperatures, see Figs. 4 and 6.

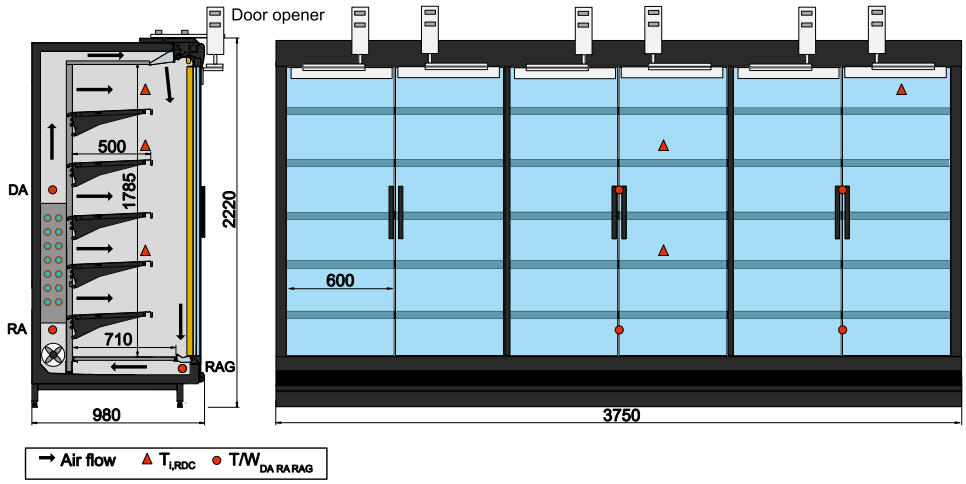

Fig. 2. Drawing of the RDC used for the validation experiment where locations for sensors are indicated together with the dimensions of the RDC. The three triangles represent the thermocouples located in the gross volume of the RDC. The circles represent the position of the temperature and humidity sensors, located in the duct before and after the heat exchanger in the back.

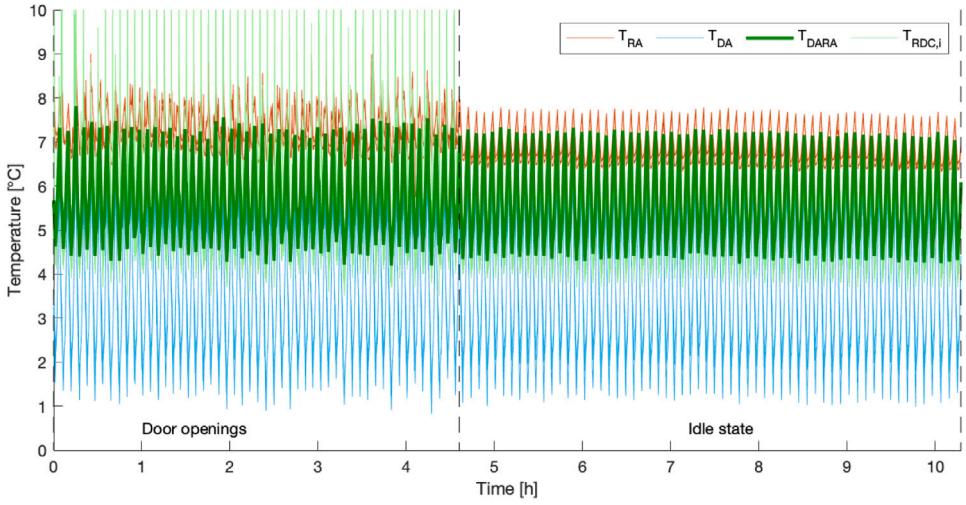

Fig. 3. Temperature overview for the full duration of the experiment. The larger variations during the first 4 h 35 min are caused by the door operations. Later, the RDC was left at idle state, allowing the temperature to stabilise.

3.1. Boundary conditions and input parameters

Table 1 presents the boundary conditions and performance parameters used for the validation. The values for K_{Env}, $\dot{m}_{Idle}$ and $m_{Opening}$ were found by performing the Co-Heating test series following the methodology presented in [39].

3.2. Validation of temperatures

For the period with the RDC at idle state, the measured mean return air temperature was 6.94/7.02 °C in the centre and the right section of the RDC, respectively, whereas the calculated value was slightly higher, that is 7.12 °C. The standard deviation for the measured values during the same period was 0.40/0.33 °C compared with the calculated value of 0.56 °C. Considering the accuracy of the temperature sensors and the stochastic errors by the control system, the results are showing good conformity. Moreover, for the period of door openings, the model is showing good conformity, as shown in Table 2.

Fig. 4 shows a more detailed view of the temperature variations taken 4 h after the door operations were stopped. Here, the span of temperature variations and compressor cycling times of the model corresponds well with the experiment. As shown, the estimated T_{DARA} follows both the measured T_{DARA} and the two measurement points in the RDC display volume, $T_{RDC,i}$. The calculated return air temperature, $T_{RA,Model}$, varies between 6.2 and 8.0 °C in the model whereas the measured T_{RA} has a slightly narrower span, between 6.4 to 7.7 °C.

The calculated discharge air temperature does also follow the measured values with good conformity. During the cooling cycle, the lowest calculated temperature is approximately 0.5 °C higher than the lowest measured temperature.

Table 2
Mean, median and standard deviation of temperature variations for Return air and Discharge air temperature, as calculated by the model and measured during the experiment.

	Return air (T_{RA})			Discharge air (T_{DA})		
	Mean	Median	STD-dev	Mean	Median	STD-dev
No Openings						
Model	7.12	7.16	0.56	4.18	4.29	1.34
Experiment	6.94/7.02	6.89/6.99	0.40/0.33	3.44/3.73	3.24/3.52	1.42/1.18
6 openings h^{-1}						
Model	7.01	7.01	0.72	3.68	3.91	1.34
Experiment	7.37/7.47	7.3/7.41	0.45/0.44	3.36/3.54	3.10/3.40	1.36/1.18

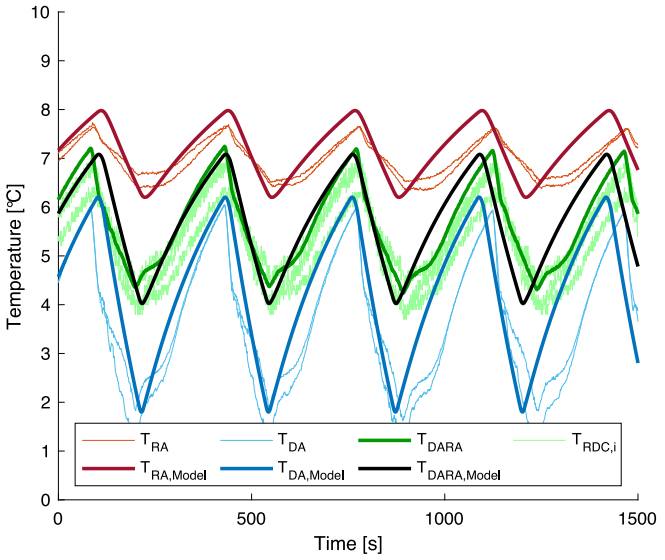

Fig. 4. Closer view taken 8 h 45 min after the start of the experiment, which shows the temperature variations in the RDC at idle state (Doors closed), simulated in *Thermostat-mode*.

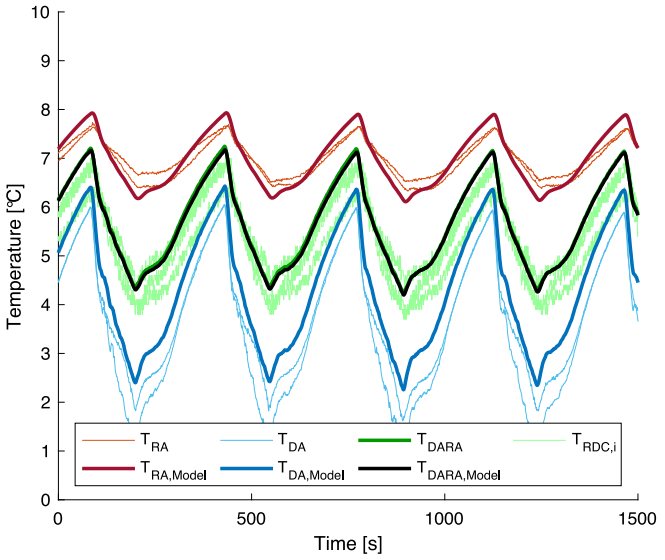

Fig. 5. Closer view taken 8 h 45 min after the start of the experiment, which shows the temperature variations in the RDC at idle state, both measured and as calculated with the model in Input-controlled mode. Here with the measured T_{DARA} as input for the control system.

The model was also validated in *Tracking-mode* where it was set to follow the measured T_{DARA} temperature. Based on the difference between the calculated and measured values of T_{DARA}, the magnitude of the fictitious heat sink from Eq. (15) was adjusted at every time step. Thereafter, a new evaporator temperature is evaluated as defined in Eq. (14). Finally, the dependent variables are evaluated based on the heat extraction caused by the evaporator domain as described in Eqs. (9)–(13). In Fig. 5, the measured and calculated temperatures are shown from the same period as in Fig. 4. Unlike Fig. 4 the measured and calculated T_{DARA} are overlaying in this case, confirming that the control strategy applied in the model is adequate. By following the measured T_{DARA}, the earlier explained time lags due to irregular operation of the compressor are avoided, although some differences do exist. The return air temperature amplitude of the model is approximately 0.1 °C higher than the measured, whereas the mean return air temperatures

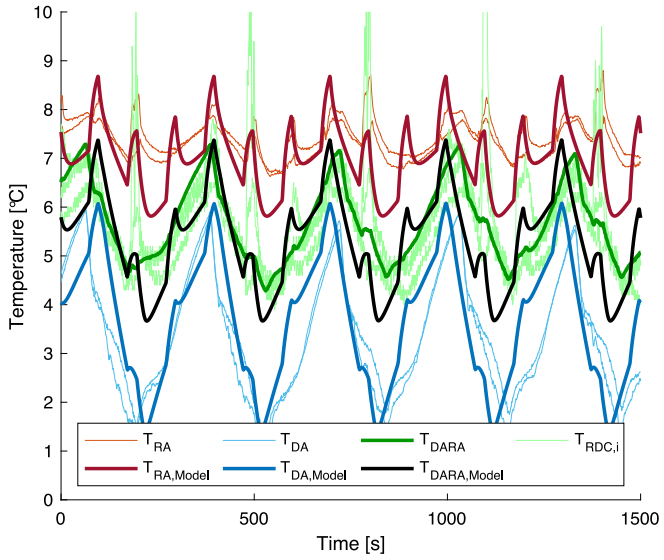

Fig. 6. Closer view taken 2 h 54 min into the validation experiment, with doors operated 6 times per hour per door. The generally larger variations in temperature and local smaller peaks represent the effects of door openings. The calculated temperatures and cycle time with the model in *Thermostat-mode* show good conformity with the measured values.

are equal for both the model and the experiment. Furthermore, the calculated mean discharge air temperature is 0.74/0.45 °C higher than that of the measured temperature. This is partly a consequence of the time-lag and thermal inertia, which affects the air from when it leaves the evaporator to when it affects the T_{DARA} measurement, which is used as input for the model.

For the period when door operations were present, both the measured and calculated temperatures vary significantly more than at the idle state, as shown in Fig. 6. The calculated T_{DARA} shows more pronounced discrepancies from the measured values. In addition, the local peaks caused by the warm infiltrating air coming through the opened doors are slightly more prominent in the model than the measured T_{DARA}. The change registered in the measured temperature in the gross volume, $T_{RDC,i}$, is conversely significantly larger for some door openings. This is due to the local position of the thermocouple in the RDC where it responded almost instantly to the infiltrating air, whereas the modelled thermal inertia of the RDC limits the change of T_{DARA}.

Fig. 7 presents the results from the model ran in *Tracking-mode* over the same period. Here, the calculated values are showing better conformity with the measurements. There are, however, some significant discrepancies in the momentary calculated discharge air temperature, which is a consequence of over-compensation by Q_{Adjust} for the discrepancies that were visible in *Thermostat-mode*.

As shown in Fig. 6, the local peaks caused by door openings are more prominent in the model than in the measured T_{DARA}. Consequently, in *Tracking-mode*, when the model is forced to follow the measured T_{DARA}, the calculated heat exchanger temperature responds to smooth the temperature(T_{DARA}), thereby the discrepancies in the discharge air.

Furthermore, for the return air, the calculated and measured temperatures are showing good conformity. The local peaks are slightly more prominent and the mean temperature is approximately 0.2 °C lower.

3.3. Duration of refrigeration cycles and temperature change rate

Another aspect that shown in Fig. 6 is that the refrigeration cycles are slightly shorter in the model than in the experiment. To visualise this variation in cycle duration, Fig. 8 plots the duration of cool down

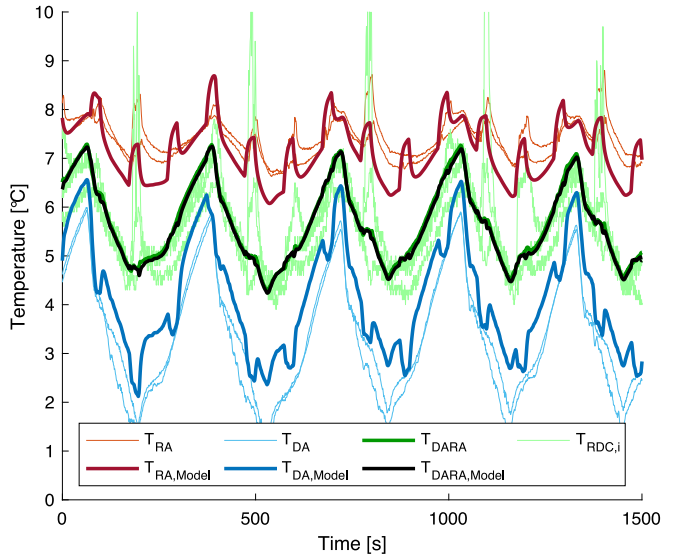

Fig. 7. Closer view taken 2 h 54 min into the validation experiment, with door operated 6 times per hour per door. The model operated in *Tracking-mode*, following the measured T_{DARA} as input. Although, there is a good conformity between calculated and measured temperatures, a slight over-prediction of lowest temperatures is shown, possibly due to time-lag.

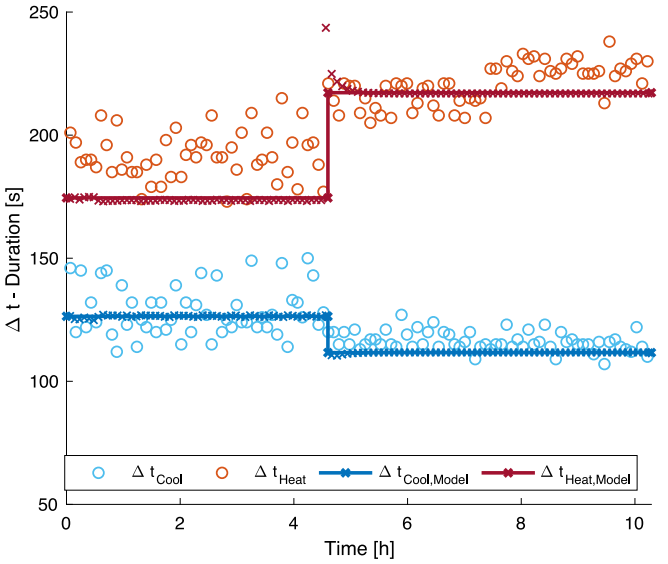

Fig. 8. The calculated and measured durations of heating and cooling cycles during the experiment, with operated doors (until 4 h 35 min) and at idle state (until 10 h 20 min). The modelled cycling times (red and blue lines) are constant and only shifted step-wise once the door operations stopped, whereas the measured cycling times vary significantly over the full duration of the experiment. The magnitude of the calculated values corresponds well with that of the measured values.

and heating period for each refrigeration cycle. The duration of the heating periods while the doors are operated is estimated to 177–178 [s] by the model compared with a larger range, i.e. between 173–215 [s] in the experiment. The duration of the cooling part of the refrigeration cycle while the doors are operated is 122–123 [s] in the model compared with 115–151 [s] in the experiment. When the RDC is at idle state, without openings, the cooling duration decreases slightly because of the decreased thermal loads, i.e. to 112.8 [s] in the model compared with a range between 110–123 [s] in the experiment. For the same reason, the heating time increases significantly, to 216 [s] in the model and a range between 207–233 [s] in the experiment.

As shown in Fig. 8, the model generally under-predicts the heating duration when the doors are operated. However, notably, the measured cycling times during the same period varied substantially, most probably due to stochastic errors in the measurements or lag in the controls, which were not considered in the model.

Another way to compare the accuracy of the prediction without the interference of the control system is to use the temperature change rate $\delta T_{DARA}/\delta t$ over each cooling or heating cycle. As shown in Fig. 9, the temperature change rate is almost constant during each separate scenario. As expected, it is slightly higher while the doors are operated compared with when the RDC is at idle state. In contrast to the measured trend, the calculated temperature change rate is slightly faster for the cooling when the doors are operated. This is a consequence of the ideal refrigeration system that is applied in the model. As the refrigeration capacity is constant, the heat exchanger temperature in the model decrease with the duration of the cooling cycle, resulting in an increased heat extraction rate and therefore a faster temperature change rate.

3.4. Validation of heat extraction

Besides the temperatures, the model also calculates the heat extraction rate of the RDC. Fig. 10 shows the accumulated extracted energy. The model estimates 35.85 $[MJ]$ to have been extracted during the period when the doors were operated, which is 4% higher than the measured value of 34.51 $[MJ]$. During the period where the RDC is at idle state, the model estimates that 37.96 $[MJ]$ was extracted compared with 37.83 $[MJ]$ as measured during the experiment, i.e. a marginal

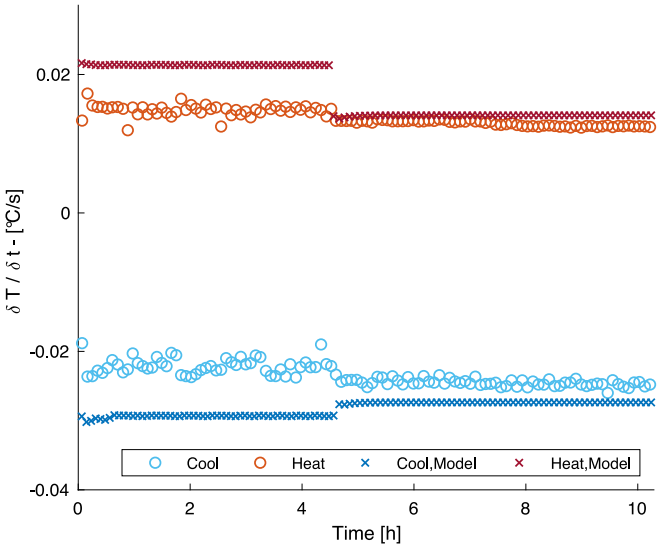

Fig. 9. Temperature decrease and increase rate for the RDC during the validation experiment. The model slightly over-predicts the temperature increase and decrease rates during the period of door openings. At idle state, the model shows good conformity with the measured values.

difference of 0.3% only. For the full duration of the experiment, the total measured extracted energy was 72.34 $[MJ]$, which is 2% lower than the calculated value of 73.81 $[MJ]$.

For the model run in *Tracking-mode* following the measured T_{DARA}, the accumulated extracted energy while the doors were operational is estimated to be 34.85 $[MJ]$ and 37.95 $[MJ]$ at idle state, which are both within 1% of the measured quantities. This indicates that the thermal loads for the RDC are correct and that the noted discrepancies between the measured and calculated results are from the stochastic errors caused by the control system.

Fig. 10 also shows the measured and calculated 15 min average heat extraction rate for the complete test period. As shown, the variations in the model are significantly smaller than the variations in the

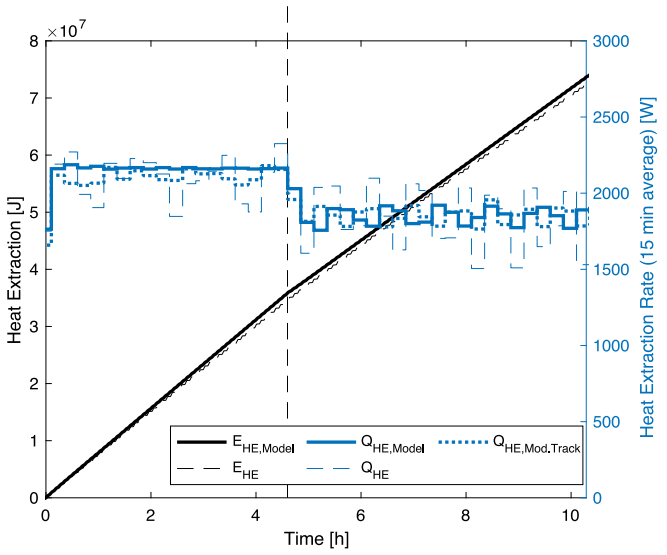

Fig. 10. Accumulated heat extraction energy during the experiment. A slightly steeper gradient during the period of door openings indicating an increased heat extraction rate during this period.

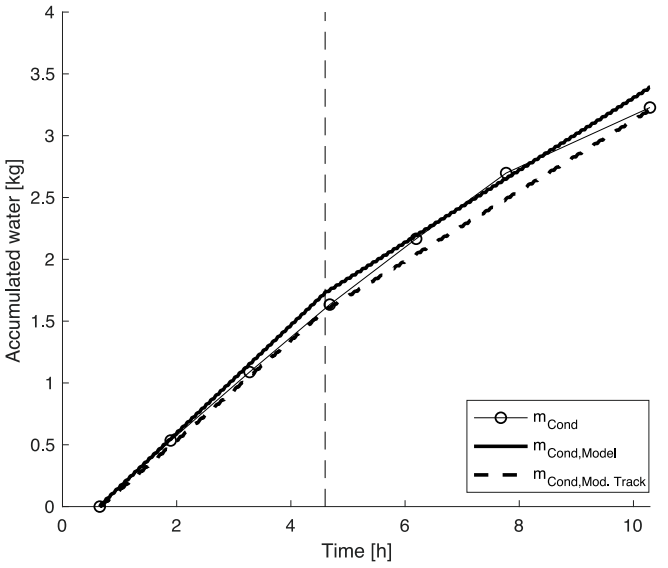

Fig. 11. Accumulated condensate water during the experiment. Measurement starting reference point at 40 min into the experiment period due to the measurement strategy chosen in the experiment.

experiment. When the model is running in *Thermostat-mode*, the heat extraction is stable over the periods, as expected. However, when ran in Input-control mode, the model inherits the errors from the control system in the experiment and shows the results with larger variations. The ambient conditions were stable at 24 °C during the time of the door openings and then increased by 1 °C when the doors were left closed. Hence, this shift should not have affected the 15-*min* mean heat extraction rate. Instead, it is likely that inaccuracies and underlying control strategies in the control system cause these variations. Some parts of the variations are a consequence of the fact that the heat extraction has a periodicity of 5 min, i.e. if the 15 min average period is including parts of a cooling-cycle it would be slightly higher.

3.5. Validation of condensation

The amount of water vapour condensing in the RDC is also calculated in the model, based on the de-humidification by the heat exchanger. Analogous to the extracted energy, the total accumulated amount of water from the RDC was calculated and compared with the measured amount, as shown in Fig. 11. As mentioned previously, the system for measuring the water from the RDC was triggered by the floating switch when approximately 500 ml of water was accumulated, which was then evacuated through the flow meter where the volume was measured more precisely. Therefore, to compare the results, the zero-reference value was chosen to be the first measuring point in the period of door openings, i.e. 40 min into the experiment.

During the remainder of the period with door openings, a total accumulation of 1.735 [kg] was estimated by the model ran in *Thermostat-mode* compared with the measured quantity of 1.601 [kg]. Hence, the model does over predict the amount of condensate water during the period of door openings by 8% in this mode. While if instead being operated in *Tracking-mode*, the estimated mass of accumulated water was 1.585 [kg], which is only < 1% higher than the measured quantity. During the following period where the RDC is left idle, the model ran in *Thermostat-mode* estimated the accumulated condensate mass to be 1.653 [kg] compared with the measured value of 1.626 [kg], which corresponds to an over-prediction of 1.6%, for the full period. Finally, for the same period but in at *Tracking-mode*, the model estimated the accumulated condensate to be 1.625 [kg], which is a negligible difference from the measured quantity. However, note that the error does vary within the period for the model ran in both modes. This is due to the fact that the accumulation of condensation is accounted for instantly in the model, whereas in the RDC there is a certain time lag between the condensation, drip off from the evaporator, measurement by the evacuation pump and flow meter. The validation does however confirm that the model is predicting the total accumulation of condensation accurately over the experimental period. Hence, since the condensation is a consequence of the infiltration rate and the air moisture conditions, the well-aligned results indicate that the infiltration process is accurately depicted in the model.

3.6. Sensitivity analysis

In general, the results from the model are showing good conformity with those from the validation experiment. Errors in the results due to simplifications in the model, in input data, and the inaccuracy of the measuring equipment are expected. In this section, the input parameters are varied to evaluate how each parameter affects the results.

The ambient conditions were varied to represent the uncertainties in the measurements during the validation experiment, i.e. ±1 °C and ±2% RH. The infiltration rate was evaluated following the Co-heating method described in [39]. To accommodate for any errors in these tests, the infiltration rate was varied ±10% for both the constant infiltration through the gaps ($\dot{m}_{Inf,0}$) and the time-varying infiltration caused by door openings ($\dot{m}_{Inf,Opening}$).

As shown in Table 3, the variation in infiltration through the gaps affects the evaluated parameters significantly more than the variation in infiltration by door openings. Furthermore, a measurement error or change in the ambient temperature of ±1 °C would influence the heat extraction by approximately ±7% and the amount of condensate would be affected by almost ±20%. In analogy, a change in RH by ±2% would affect the amount of condensed water with ±15–17% and the heat extraction rate by approximately ±2%.

4. Parametric study on refrigeration cycle time

By reducing the electrical power demand for refrigeration, the supermarket could assist in balancing the grid. As the introduction

Table 3
Results from sensitivity study of RDC model where parameters for ambient conditions and infiltration was varied.

		Original	−1°C	+1°C	RH −2%	RH +2%	Inf −10%	Inf +10%	Door −10%	Door +10%
$T_{RADA,Idle}$	[° C]	5.66	5.66 (0.1%)	5.67 (0.2%)	5.67 (0.2%)	5.66 (0.1%)	5.67 (0.2%)	5.66 (0.1%)	5.66 (0.0%)	5.66 (0.0%)
$T_{RADA,Door}$	[° C]	5.35	5.49 (2.7%)	5.46 (2.1%)	5.32 (−0.5%)	5.40 (1.0%)	5.29 (−1.1%)	5.43 (1.5%)	5.36 (0.3%)	5.36 (0.3%)
$\Delta t_{Cooling,Idle}$	[s]	111.6	110.5 (−1.1%)	115.2 (3.2%)	110.7 (−0.8%)	112.7 (0.9%)	110.9 (−0.7%)	114.6 (2.6%)	111.7 (0.0%)	111.6 (0.0%)
$\Delta t_{Cooling,Door}$	[s]	126.4	120.0 (−5.1%)	128.0 (1.3%)	125.4 (−0.8%)	125.2 (−0.9%)	125.1 (−1.0%)	126.7 (0.2%)	124.6 (−1.4%)	126.6 (0.1%)
$\delta T_{Cool,Idle}/\delta t$	[° C/s]	−0.0300	−0.0307 (2.3%)	−0.0291 (−3.0%)	−0.0302 (0.9%)	−0.0297 (−0.9%)	−0.0306 (2.1%)	−0.0292 (−2.7%)	−0.0300 (0.0%)	−0.0300 (0.0%)
$\delta T_{Cool,Door}/\delta t$	[° C/s]	−0.0250	−0.0283 (13.2%)	−0.0247 (−1.2%)	−0.0253 (0.9%)	−0.0253 (1.0%)	−0.0255 (1.7%)	−0.0250 (−0.2%)	−0.0254 (1.6%)	−0.0248 (−1.1%)
$\Delta t_{Heating,Idle}$	[s]	217.25	231.20 (6.4%)	202.76 (−6.7%)	221.68 (2.0%)	213.01 (−1.9%)	227.48 (4.7%)	206.26 (−5.1%)	217.24 (0.0%)	217.25 (0.0%)
$\Delta t_{Heating,Door}$	[s]	174.51	203.48 (16.6%)	172.71 (−1.0%)	175.79 (0.7%)	174.36 (−0.1%)	176.28 (1.0%)	172.95 (−0.9%)	176.25 (1.0%)	174.38 (−0.1%)
$\delta T_{Heating,Idle}/\delta t$	[° C/s]	0.0145	0.0135 (−7.0%)	0.0156 (7.2%)	0.0142 (−2.1%)	0.0148 (2.0%)	0.0138 (−5.2%)	0.0153 (5.2%)	0.0145 (0%)	0.0145 (0%)
$\delta T_{Heating,Doors}/\delta t$	[° C/s]	0.0187	0.0163 (−13.1%)	0.0198 (5.5%)	0.0184 (−1.8%)	0.0191 (1.9%)	0.0181 (−3.4%)	0.0193 (2.8%)	0.0183 (−2.0%)	0.0192 (2.6%)
$m_{Cond,Idle}$	[g/s]	0.0810	0.0642 (−20.8%)	0.0986 (21.8%)	0.0666 (−17.8%)	0.0955 (17.9%)	0.0713 (−12.0%)	0.0908 (12.2%)	0.0810 (0.0%)	0.0810 (0.0%)
$m_{Cond,Door}$	[g/s]	0.1219	0.0943 (−22.7%)	0.1433 (17.5%)	0.1036 (−15.1%)	0.1384 (13.5%)	0.1119 (−8.3%)	0.1302 (6.8%)	0.1180 (−3.3%)	0.1260 (3.4%)
$\dot{Q}_{HE,Idle}$	[W]	1848	1725 (−6.6%)	1971 (6.7%)	1806 (−2.2%)	1883 (1.9%)	1743 (−5.6%)	1947 (5.4%)	1847 (0.0%)	1847 (0.0%)
$\dot{Q}_{HE,Door}$	[W]	2286	2135 (−6.6%)	2438 (6.7%)	2235 (−2.2%)	2330 (1.9%)	2157 (−5.6%)	2408 (5.4%)	2286 (0.0%)	2286 (0.0%)

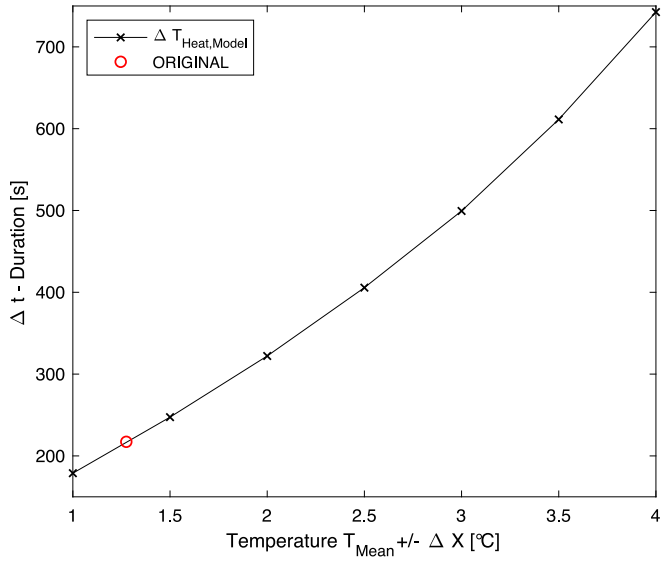

Fig. 12. Heating duration for the RDC plotted against the allowable temperature limits, to account for different types of stored goods. By increasing the allowable temperature range, the heating duration increases. The original allowed temperature range was 1.275 °C.

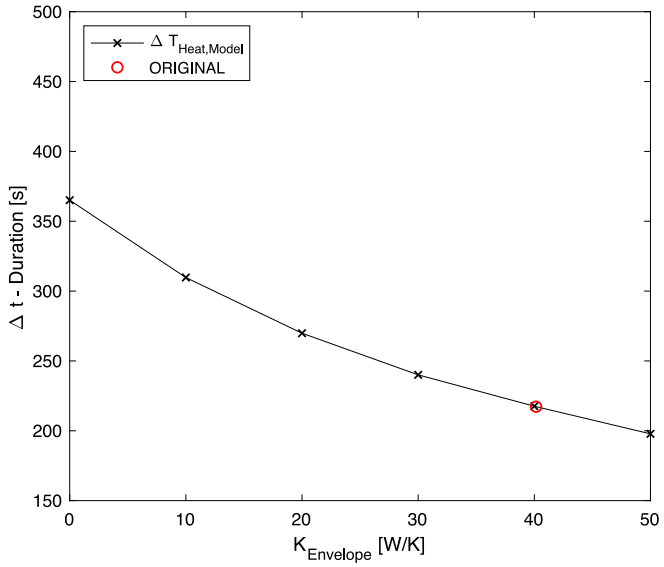

Fig. 13. Heating duration for the RDC with respect to overall heat transfer coefficient of its envelope. An infinitely isolated RDC envelope would require 365 s to heat up, compared with 217 s in its original appearance.

presents, the demand response capacity of an RDC is ultimately depending on the duration for which it can be operated without requiring any active heat extraction. Thus, the longer the heating period is, the larger the flexibility for load shifting in the electrical grid. To gain further insights in how adjustable variables affect this issue, a parametric study on how some selected performance parameters of the RDC affect the heating duration was conducted. Within a supermarket, this flexibility could be used for load scheduling to allow the compressor to run at an optimal level, i.e. for energy efficiency measures. Where appropriate, the theoretically most favourable condition for the heating duration is included in the analysis to serve as a reference when interpreting more realistic conditions.

As a starting point, the effects of a varying accepted temperature range for the thermostat control is evaluated. Some products, such as meat, are more sensitive to temperature variations whereas other products, such as cold beverages, have a larger accepted range of temperature variations. Hence, the heating duration would be expected to increase with the larger accepted temperature range. This is confirmed in Fig. 12 where the $\Delta t_{Heating}$ is plotted towards accepted temperature span, assuming a mean temperature in the RDC set to 6 °C.

As shown, the time it takes to heat from T_{Min} to T_{Max} increases significantly as the difference between the two increases. For the RDC in the setup as in the validation experiment, the accepted temperature variations were ±1.275 °C, resulting in a heating duration of 217 s. This heating duration would have increased by 48% to 322 s if the control system allowed variations of ±2 °C, or as high as 742 s if ±4 °C is allowed, which could be the case for less sensitive products such as sodas etc.

An area that has gained a lot of attention when developing energy-efficient RDCs is the thermal transmittance of the walls and doors, which defines the heat transfer coefficient of the RDC. For an infinitely insulated RDC, the heat transfer coefficient of the envelope, K_{Env} = 0 [W/K], i.e. no heat losses through the envelope. Such ideal RDC would still heat up due to infiltration, which results in a heating duration of 365 s. The heat extraction rate would, however, decrease by 41% for the case of the RDC at idle state under the same conditions as used in the validation experiment. By contrast, in case the thermal heat transfer coefficient increases to 50 [W/K] due to the degradation of insulation materials, the heating duration decreases by 19.5 s and the needed heat extraction increases by 10% for the scenario with no door openings. Fig. 13 plots the heating duration for a parametric sweep of K_{Env} between 0 to 50 [W/K].

Another aspect that significantly affects the thermal loads and, thereby, the heating duration is the infiltration of ambient air. In an ideal RDC, there would be no infiltrating air, which would have resulted in a decreased heat extraction rate by 51%. In addition, the heating duration would have increased to 442 s as shown in Fig. 14 where the heating duration is plotted towards the infiltration rate.

Another approach to increase the time it takes for the RDC to heat up is to increase its active thermal mass. To evaluate this effect, the thermal capacity of the heat exchanger was adjusted to represent a mass increase of 0–100 [kg] or in terms of increased heat capacity of

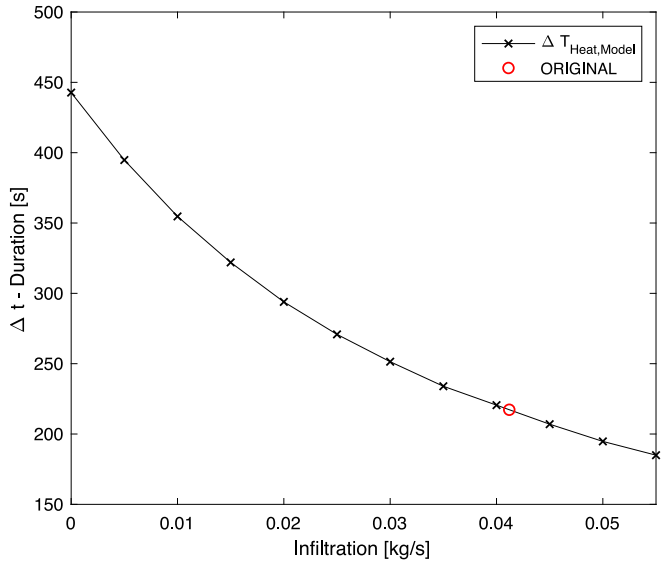

Fig. 14. Heating duration for the RDC with respect to the air infiltration through the gaps in the envelope. An airtight RDC would take significantly longer time to increase its temperature than the original design.

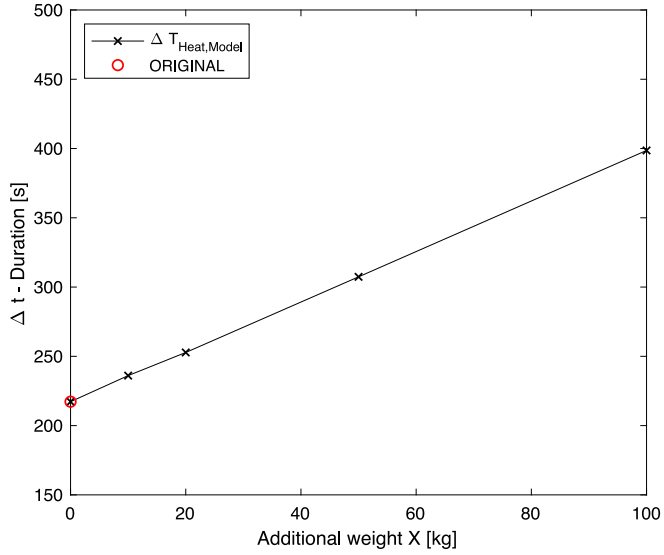

Fig. 15. Heating duration for the RDC plotted towards the relative increase of active thermal mass, modelled as an additional mass of the heat exchanger.

0–64250 [J/K]. As shown in Fig. 15, the heating duration in this case increases by approximately 1.8 [s/kg].

As demonstrated above, the thermal performance of an RDC affects significantly the heating duration and, consequently, the demand response capacity of the refrigeration system. Further details, analysis and optimisations of these parameters are important future directions for the development of topics for supermarkets, as resources for demand response. This is, however, beyond the scope of this article.

5. Using the model to estimate available flexibility

In the validation section, it was concluded that the model estimates the temperatures and heat extraction rate with good conformity both in *Tracking-mode* and *Thermostat-mode*. By using live temperatures from an RDC, the model can be used to predict the near future temperature for different scenarios that the RDC could be exposed to in operational

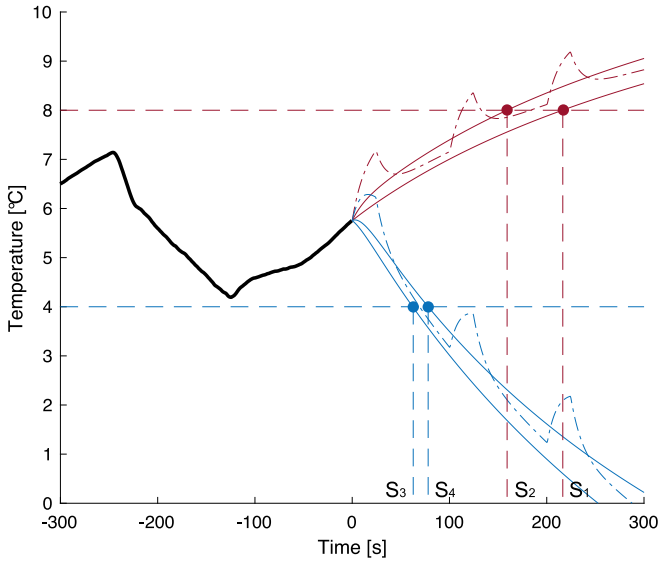

Fig. 16. Plot showing the temperature development for T_{DARA} for the RDC exposed to Scenario 1–4. Here it can be seen that it takes 159–217 s for the RDC to heat to 8 °C, or 59–74 s to cool to 4 °C. The dash-dotted line shows the temperature development including the temporal effects of door openings.

conditions. For example, the heating duration can be predicted or the time required to cool the RDC from the current temperature to a lower level. By knowing this information, the control system of the refrigeration system could optimise the scheduling of cooling cycles or estimate how long the system could be operated at reduced electrical power. The latter can be utilised as a demand response resource in a smart grid.

Fig. 16 shows an example of the prediction by the model. Here, the solid black line represents the historical measured T_{DARA} from the validation experiment, which the model has used as input in *Tracking-mode* until time 0. At time 0, the model is switched to *Thermostat-mode* with four scenarios:

- S_1 - No openings, No Cooling
- S_2 - 6 openings per door per hour, No Cooling
- S_3 - No openings, Active Cooling
- S_4 - 6 openings per door per hour, Active Cooling

Based on the results from the simplified case of the four scenarios presented above, it is shown that if the refrigeration system could be turned off at time 0, it would take between 159–217 s to heat up the RDC to the upper limit of the accepted temperature range, T_{Max}, or it would take 59–79 s to cool down from the current temperature level to the lower limit of the acceptable temperature range, T_{Min}. The dash-dotted lines are showing the temperature development including the sudden change caused by door openings for S_2 and S_4. As shown for the line representing S_2, the door openings cause the temperature to cross the upper limit at 114, 132 and 185 s. Therefore, the infiltration caused by the door openings was averaged to generate a representative trace for the temperature development when the door openings were active.

The number and variations of scenarios can be increased, if this model would, for example, be combined with a shopping prediction model or similar. In the example presented in Fig. 16, the simulations were conducted on a MacBook A1980 with 2.3 GHz Quad-Core Intel Core i5 with 16 GB RAM, which results in a total calculation time of less than 0.5 s for all scenarios, i.e. the model prediction could be updated at a frequency of 2 [Hz] for four alternative scenarios. Notably, the simulation time includes the initialisation of the MatLab SimuLink-model, i.e. the calculation time per variation would be drastically decreased for additional scenarios or multiple RDCs.

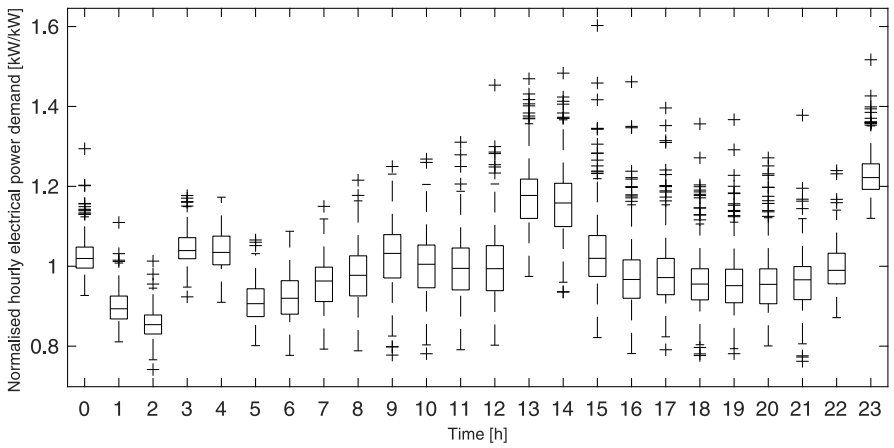

Fig. 17. Normalised daily electrical power demand profile by the medium temperature refrigeration in a 1300 m^2 supermarket in Germany. The values are normalised to the annual mean power demand of 15.17 kW. The data are from annual power demand with an hourly granularity, sorted by time of day and presented in a box plot.

6. Discussion: Hypothetical application of the model in an operational supermarket

The presented model has been developed to examine and enable supermarkets to act as a resource for demand response and assist in balancing the electrical grid. In this section, the model is applied to a hypothetical supermarket, created to simulate an actual supermarket.

Fig. 17 shows the hourly variation of power-demand for medium temperature (2–6 °C) refrigeration over a day, normalised to the annual mean (15.17 [kW]) for the 1 300 m^2 actual supermarket, used as reference. As shown, the power demand is approximately 10–20% below average during mornings and evenings, whereas it is 15–25% above average just after noon. At 23:00 there is a defrost event, causing several RDCs to have an increased heat extraction demand to compensate for the over-temperatures indicating 50% higher power demand than the annual average. Based on the highest recorded hourly power demand, which is approximately 60% higher than the average, the rated power of the compressors is at least in this magnitude.

This implies that in case of excess energy in the electrical grid, the supermarket could absorb electricity by running the compressors at their rated power demand until the RDCs have reached their lower temperature limit, T_{Min}. Alternatively, at times of energy deficiency in the grid, the supermarket could potentially decrease its power demand to near-zero, for the duration it takes for the RDCs to heat up to the upper temperature limit, T_{Max}.

It should be explicitly mentioned that the selected supermarket in the presented example is equipped with RDCs of the same brand and model as the one used for validation in this study, making it suitable as a reference. Within the supermarket, there are, however, 62 doors distributed over 15 RDC modules, i.e. some modules are shorter than the one used for validation.

To illustrate how the model can be used to evaluate the potential demand response of a supermarket, a hypothetical supermarket with 11 RDC modules identical to the one used for the validation within this study was constructed, i.e. a total of 66 doors.

In the hypothetical example, it is assumed that the supermarket operates all RDCs as in the validation experiment with a temperature set-point range of $T_{DARAG,Set}$ = 4.85–7.40 °C. Then, at the time of the demand response signal, the control system widens the range of accepted temperatures to $T_{DARA,Set}$ = 4–8 °C. The initial conditions of the RDCs are taken from a measured refrigeration cycle where T_{DARAG} varied between 4.25–7.00 °C, which is analogous to the input data used in the example presented in Fig. 16.

Assuming that the RDCs are evenly distributed in time in their individual refrigeration cycles, then 4 (34%) of the RDC would be actively cooling and 7 (66%) of the RDCs would be passively heating up. By applying the four scenarios, namely S_1–S_4 mentioned above, we can estimate the number of RDCs that would require active cooling at a given time after a demand response signal to turn off the refrigeration system; or, alternatively, for what duration the compressors could be operated at increased power. Fig. 18 shows, the result of a simulation with the four scenarios.

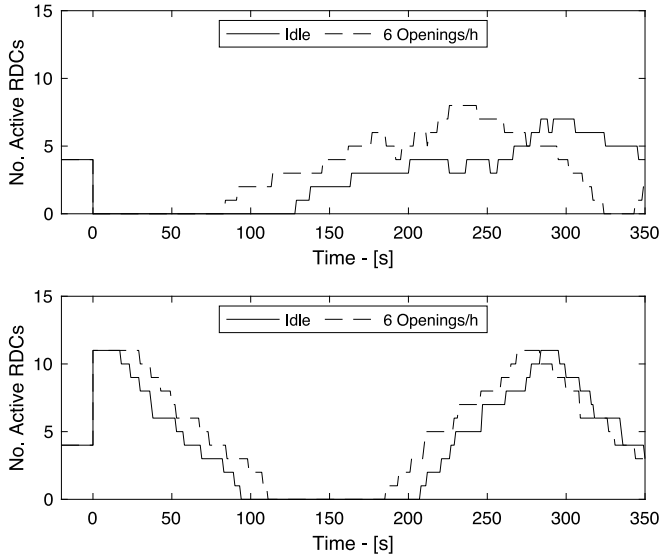

Fig. 18. *Top*: Number of active RDC at a specific time after a demand response signal to reduce power demand. *Bottom*: Number of active RDCs after a demand response signal to increase power demand to absorb energy.

In the upper figure, the response to a request to lower the power is shown. At idle state, S_1, the RDCs could be kept off for 127 s before the warmest RDC requires active cooling again, whereas at the scenario, $S2$, with 6 door openings per door, the request would come already after 83 s. The cooling demand then gradually increases as more and more RDCs are reaching the upper limit of 8 °C. Finally, it culminates when 7 (S_1) / 8(S_2) RDCs simultaneously request active cooling.

For the case of a demand response signal requesting the supermarket to absorb energy, all RDCs could be activated and would be able to run at full power for 17 s at idle state, S_3, or 29 s as in the case of doors being operated as in S_4, before the coldest would have reached the lower limit of 4 °C. However, 8 or more RDCs could be active for 33 / 47 s before the lower limit is reached, contributing to a 50% increased heat extraction demand.

In the scenarios presented above, the RDCs are only controlled individually by a thermostat control script that activates and de-activates the refrigeration for the individual RDC based on the temperature limits and the RDCs current temperature. Through the implementation of more sophisticated algorithms for control, the heat extraction rate demand curve could be manipulated to benefit the grid better. For example, the valley of zero active RDCs after responding to a demand response signal could be mitigated by activate cooling before reaching the upper limit. This would also help in harmonising the cooling requests and, thereby, ensuring that the compressors are operated at optimal levels.

The scenarios used in the example above are applied to all RDCs simultaneously, which is unlikely to occur in an operational supermarket during opening hours. Most likely, the door opening frequency will be intermittent with significant variations in time and between different RDCs. By contrast, during the time outside of the opening hours, the two scenarios (S_1 *and* S_3) that represents the RDC at idle state are likely to represent the supermarket adequately, giving a good indication of the demand response capacity at these times.

To further examine the demand response capacity during the opening hours, the data on door operations such as the data-set presented in [43] should be integrated, and the thermal performance data from the specific cabinets should be generated.

7. Conclusion

This work presents a computationally efficient yet accurate hygrothermal model of a refrigerated display cabinet together with a methodology to evaluate and enable demand response by supermarket refrigeration systems. The model generates results for return air, discharge air and heat exchanger temperature, as well as the mass-flow of condensate and heat extraction demand for the RDC, with a temporal granularity of seconds. Unlike other models presented in the literature, this model can depict operational conditions and customer interactions through door openings.

The model can be run in two modes, allowing near-future predictions of temperature development and heat extraction demands in the RDC (*Thermostat-mode*) or optimisation of its refrigeration strategy to benefit the electrical grid by demand response, or for energy efficiency purposes (*Tracking-mode*).

For the tested RDC, with a set-point temperature at approximately 7 °C, the difference between the measured and calculated mean return air temperature was less than 0.2 °C at idle state, and less than 0.4 °C when doors were operated. The accumulated heat extraction was predicted with an accuracy of 2% over the full length of the experiment in (*Thermostat-mode*), and estimated with an accuracy of < 1% when the model was set to follow the temperature of the RDC (*Tracking-mode*). Considering the accuracy of the temperature sensors and the stochastic errors by the control system, the results are showing good conformity.

From the generated results, it was found that the demand response capacity can be significantly increased by reducing the amount of infiltrating air or increasing the available thermal mass within the RDC. It was also found, based on the results from the model applied to a hypothetical supermarket, that there exists a potential capacity to reduce the heat extraction demand to zero for 127 s during non-opening hours of the supermarket. Alternatively, if all RDCs would be pre-cooled to its lower set-point (4 °C) prior to the demand response request, the refrigeration system could instead be turned off for up to 322 s. In both cases, the combined demand response capacity of supermarkets on a national level would be significant. For the mentioned example of Germany in the introduction, it would be in the magnitude of 570 MW.

The model was able to generate a complete 5-min ahead forecast of all parameters of interest for the RDC at four variations of the operation scenarios, in less than 0.5 s. Thus, the model is found suitable for integration in control systems to enable control strategies based on forecasting for demand response purposes and energy efficiency.

Future work is, however, required to further evaluate the capacity of operational supermarkets and for the integration of the predictive model for optimising the refrigeration strategies.

CRediT authorship contribution statement

Tommie Månsson: Conceptualization, Methodology, Software, Validation, Writing - original draft, Visualization, Project administration. **Angela Sasic Kalagasidis:** Writing - review & editing, Supervision. **York Ostermeyer:** Supervision, Funding acquisition.

Declaration of competing interest

The authors declare that they have no known competing financial interests or personal relationships that could have appeared to influence the work reported in this paper.

Acknowledgement

The authors would like to acknowledge and thank the main funding body, EIT Climate-KIC, that has provided not just the necessary funds but also an invaluable network and inspirational community.

References

[1] European Commission. Roadmap 2050. Policy 2012;001(April):1–9. http://dx.doi.org/10.2833/10759, URL http://www.roadmap2050.eu/, arXiv.
[2] Comission E. European Comission - Renewable energy directive. 2018, URL https://ec.europa.eu/energy/en/topics/renewable-energy/renewable-energy-directive.
[3] Deloitte. European energy market reform Country profile : Germany contents. Tech. rep., Zurich: Deloitte Conseil; 2015, URL https://www2.deloitte.com/content/dam/Deloitte/uk/Documents/energy-resources/deloitte-uk-market-reform-germany.pdf.
[4] Chang MK, Eichman JD, Mueller F, Samuelsen S. Buffering intermittent renewable power with hydroelectric generation: A case study in California. Appl Energy 2013;112:1–11. http://dx.doi.org/10.1016/j.apenergy.2013.04.092.
[5] Spiliotis K, Ramos Gutierrez AI, Belmans R. Demand flexibility versus physical network expansions in distribution grids. Appl Energy 2016;182:613–24. http://dx.doi.org/10.1016/j.apenergy.2016.08.145.
[6] Wang X, Palazoglu A, El-Farra NH. Operational optimization and demand response of hybrid renewable energy systems. Appl Energy 2015;143:324–35. http://dx.doi.org/10.1016/j.apenergy.2015.01.004.
[7] Aghaei J, Alizadeh MI. Demand response in smart electricity grids equipped with renewable energy sources: A review. Renew Sustain Energy Rev 2013;18:64–72. http://dx.doi.org/10.1016/j.rser.2012.09.019.
[8] Kohlhepp P, Harb H, Wolisz H, Waczowicz S, Müller D, Hagenmeyer V. Large-scale grid integration of residential thermal energy storages as demand-side flexibility resource: A review of international field studies. Renew Sustain Energy Rev 2019;101(September 2018):527–47. http://dx.doi.org/10.1016/j.rser.2018.09.045.
[9] Kyusakov R, Eliasson J, Van Deventer J, Delsing J, Cragie R. Emerging energy management standards and technologies - Challenges and application prospects. In: IEEE international conference on emerging technologies and factory automation. 2012, http://dx.doi.org/10.1109/ETFA.2012.6489674.
[10] Cui T, Carr J, Brissette A, Ragaini E. Connecting the last mile: Demand response in smart buildings. Energy Procedia 2017;111(September 2016):720–9. http://dx.doi.org/10.1016/j.egypro.2017.03.234.
[11] Zehir MA, Batman A, Bagriyanik M. Review and comparison of demand response options for more effective use of renewable energy at consumer level. Renew Sustain Energy Rev 2016;56:631–42. http://dx.doi.org/10.1016/j.rser.2015.11.082.
[12] D'hulst R, Labeeuw W, Beusen B, Claessens S, Deconinck G, Vanthournout K. Demand response flexibility and flexibility potential of residential smart appliances: Experiences from large pilot test in Belgium. Appl Energy 2015;155:79–90. http://dx.doi.org/10.1016/j.apenergy.2015.05.101.
[13] Li J, Fang J, Zeng Q, Chen Z. Optimal operation of the integrated electrical and heating systems to accommodate the intermittent renewable sources. Appl Energy 2016;167:244–54. http://dx.doi.org/10.1016/j.apenergy.2015.10.054.
[14] Neves D, Pina A, Silva CA. Assessment of the potential use of demand response in DHW systems on isolated microgrids. Renew Energy 2018;115:989–98. http://dx.doi.org/10.1016/j.renene.2017.09.027.
[15] Short JA, Infield DG, Freris LL. Stabilization of grid frequency through dynamic demand control. IEEE Trans Power Syst 2007;22(3):1284–93. http://dx.doi.org/10.1109/TPWRS.2007.901489.
[16] Chanana S, Arora M. Demand response from residential air conditioning load using a programmable communication thermostat. Int J Electr Comput Eng 2013;7(12):1670–6. http://dx.doi.org/10.5281/zenodo.1089330.
[17] Hovgaard TG, Halvgaard R, Larsen LFS, Jørgensen JB. Energy efficient refrigeration and flexible power consumption in a smart grid. In: Proceedings of Risø international energy conference. 2011. p. 164–75.

[18] Söyrinki S, Heiskanen E, Matschoss K. Piloting demand response in retailing: Lessons learned in real-life context. Sustain 2018;10(10):1–17. http://dx.doi.org/10.3390/su10103790, (Switzerland).
[19] Månsson T. Energy in supermarkets, vol. 1 [Licentiate thesis], Chalmers University of Technology; 2016, p. 1–72.
[20] Funder T. Supermarkets as an important smart grid application. In: 16th European conference, technological innovations in refrigeration and in air conditioning. Milan: Danfoss; 2015, p. 1–4.
[21] Statens Energimyndighet. STIL 2 - Energianvändning i handelslokaler. Tech. rep., Stockholm: Energimyndigheten; 2010, p. 1–123.
[22] Statista. Retail Week. (n.d.). Number of stores of key food and grocery retailers in Germany in 2013, by store count. In: The statistics portal. 2013.
[23] Arias J. Energy usage in supermarkets - Modelling and field measurements [Ph.D. thesis], Royal Institute of Technology; 2005.
[24] Retail Forum for Sustainability. Issue paper on the energy efficiency of stores. Retail Forum Sustain 2009;1(1):1–9.
[25] Pedersen R, Schwensen J, Biegel B, Green T, Stoustrup J. Improving demand response potential of a supermarket refrigeration system: A food temperature estimation approach. IEEE Trans Control Syst Technol 2017;25(3):855–63. http://dx.doi.org/10.1109/TCST.2016.2583958.
[26] Hviid J, Kjærgaard MB. The retail store as a smart grid ready building: Current practice and future potentials. In: 2018 IEEE power and energy society innovative smart grid technologies conference. 2018, p. 1–5. http://dx.doi.org/10.1109/ISGT.2018.8403354.
[27] Oconnell N, Pinson P, Madsen H, Omalley M. Benefits and challenges of electrical demand response: A critical review. Renew Sustain Energy Rev 2014;39:686–99. http://dx.doi.org/10.1016/j.rser.2014.07.098.
[28] Laguerre O, Duret S, Hoang HM, Flick D. Using simplified models of cold chain equipment to assess the influence of operating conditions and equipment design on cold chain performance. Int J Refrig 2014;47:120–33. http://dx.doi.org/10.1016/j.ijrefrig.2014.07.023.
[29] Wu X, Chang Z, Zhao X, Li W, Lu Y, Yuan P. A multi-scale approach for refrigerated display cabinet coupled with supermarket HVAC system – Part I: Methodology and verification. Int J Heat Mass Transfer 2015;87:673–84. http://dx.doi.org/10.1016/j.ijheatmasstransfer.2015.04.004.
[30] Wu X, Chang Z, Zhao X, Li W, Lu Y, Yuan P. A multi-scale approach for refrigerated display cabinet coupled with supermarket HVAC system-Part II: The performance of VORDC and energy consumption analysis. Int J Heat Mass Transfer 2015;87:685–92. http://dx.doi.org/10.1016/j.ijheatmasstransfer.2015.04.003.
[31] Smale N, Moureh J, Cortella G. A review of numerical models of airflow in refrigerated food applications. Int J Refrig 2006;29(6):911–30. http://dx.doi.org/10.1016/j.ijrefrig.2006.03.019, URL http://www.sciencedirect.com/science/article/pii/S0140700706000971.
[32] Orlandi M, Visconti FM, Zampini S. CFD assisted design of closed display cabinets. In: 2nd IIR international conference on sustainability and the cold chain, vol. 2. Paris: International Institure of Refrigeration; 2013, p. 1–8.
[33] Sarhadian R, Gage C, Faramarzi R. ASHRAE handbook: Refrigeration (I-P edition). 2002nd ed. Atlanta: Comstock, W. Stephen; 2002, p. 47.1–47.18, Most.
[34] Howell RH. Effects of store relative humidity on refrigerated display case performance. ASHRAE Trans 1993;99(1).
[35] Fahlén P. Refrigeration in supermarkets (SP AR 1999:09). Tech. rep., Borås: The Swedish National Testing and Reserach Institute; 1999, p. 53.
[36] Laguerre O, Hoang MH, Flick D. Heat transfer modelling in a refrigerated display cabinet: The influence of operating conditions. J Food Eng 2012;108(2):353–64. http://dx.doi.org/10.1016/j.jfoodeng.2011.07.027.
[37] Ben-abdallah R, Leducq D, Hoang HM, Pateau O, Ballot-Miguet B, Delahaye A, et al. Modeling and experimental investigation for load temperature prediction at transient conditions of open refrigerated display cabinet using Modelica environment. Int J Refrig 2018;94:102–10. http://dx.doi.org/10.1016/j.ijrefrig.2018.02.017.
[38] Chaomuang N, Laguerre O, Flick D. Dynamic heat transfer modeling of a closed refrigerated display cabinet. Appl Therm Eng 2019;161(March 2019):114138. http://dx.doi.org/10.1016/j.applthermaleng.2019.114138.
[39] Månsson T, Kalagasidis AS, Ostermeyer Y. Co-Heating method for thermal performance evaluation of closed refrigerated display cabinets. Int J Refrig 2020. http://dx.doi.org/10.1016/j.ijrefrig.2020.10.011, URL http://www.sciencedirect.com/science/article/pii/S0140700720304217.
[40] Faramarzi RT, Coburn BA, Sarhadian R. Performance and energy impact of installing glass doors on an open vertical deli/dairy display case. ASHRAE Trans 2002;108 PART 1:673–9.
[41] 2017 ASHRAE handbook - Fundamentals (SI-edition). 2017th ed. Atlanta: ASHRAE, American Society of Heating, Refrigerating and Air-Conditioning Engineers Inc; 2017, p. 8.
[42] International Standard Organisation. EN ISO 23953-2:2005. 2005, 121124.
[43] Månsson T, Rukundo A, Almgren M, Tsigas P, Marx C, Ostermeyer Y. Analysis of door openings of refrigerated display cabinets in an operational supermarket. J Build Eng 2019;26:100899. http://dx.doi.org/10.1016/j.jobe.2019.100899, URL https://linkinghub.elsevier.com/retrieve/pii/S235271021930292X.